Local air pollution from oil rig emissions observed during the airborne DACCIWA campaign

Vanessa Brocchi[1], Gisèle Krysztofiak[1], Adrien Deroubaix[2], Greta Stratmann[3], Daniel Sauer[3], Hans Schlager[3], Konrad Deetz[4], Guillaume Dayma[5], Claude Robert[1], Stéphane Chevrier[1], Valéry Catoire[1]

[1] Laboratoire de Physique et Chimie de l'Environnement et de l'Espace (LPC2E), CNRS – Université Orléans – CNES, 45071 Orléans cedex 2, France.

[2] LMD and LATMOS, École Polytechnique, Université Paris Saclay, ENS, IPSL Research University; Sorbonne Universités, UPMC Univ Paris 06, CNRS, Palaiseau, France

[3] Institut für Physik der Atmosphäre, Deutsches Zentrum für Luft und Raumfahrt, Oberpfaffenhofen, Germany.

[4] Karlsruhe Institute of Technology, Institute of Meteorology and Climate Research, Karlsruhe, Germany.

[5] Institut de Combustion, Aérothermique, Réactivité et Environnement (ICARE), CNRS, 45071 Orléans cedex 2, France

Correspondence to: Gisèle Krysztofiak (gisele.krysztofiak@cnrs-orleans.fr)

Abstract. In the framework of the European DACCIWA (Dynamics-Aerosol-Chemistry-Cloud Interactions in West Africa) project, the airborne study APSOWA (Atmospheric Pollution from Shipping and Oil platforms of West Africa) was conducted in July 2016 to study oil rig emissions off the Gulf of Guinea. Two flights in the marine boundary layer were focused on the floating production storage and offloading (FPSO) vessel operating off the coast of Ghana. Those flights present simultaneous sudden increases of NO_2 and aerosols concentrations. Unlike what can be found in flaring emission inventories, no increase in SO_2 was detected and an increase in CO is observed only during one of the two flights. Using FLEXPART simulations in forward trajectory mode, our study reproduced the timing of the aircraft NO_2 enhancements. We used a regional NO_2 satellite flaring inventory in the simulations, which showed an overall good estimate of flaring emission. Several sensitivity tests on the flux and the injection height were also performed to better reproduce the measurements.

1 Introduction

Crude oil extraction from offshore platforms brings raw gas mixed with oil to the surface. Gas flaring is used to dispose this natural gas. This process emits a mixture of trace gases like carbon dioxide (CO_2), carbon monoxide (CO), sulfur dioxide (SO_2), nitrogen oxides (NO_x) as well as particulate matter. Its impacts concern both the ecosystems (Nwaugo et al., 2006; Nwankwo and Ogagarue, 2011) and the air quality (Osuji and Avwiri, 2005). The pollutants can be transported into the free troposphere (Fawole et al., 2016b) or can reach coastal cities in the marine boundary layer (MBL). Flaring emissions can be derived from remote sensing techniques (Elvidge et al., 2013) by the widely used Visible Infrared Imaging Radiometer Suite (VIIRS) Nightfire satellite product (Deetz and Vogel, 2017). Oil and gas extraction activities are however uncertain in terms of emitted quantities (Tuccella et al., 2017) and direct measurements are necessary.

In Africa, most of the studies focused on the environmental impact of Nigerian oil platform emissions (e.g. Anomohanran, 2012; Hassan and Kouhy, 2013; Asuoha and Osu Charles, 2015; Fawole et al., 2016a) as it is part of the five countries with the highest flaring amounts (Elvidge et al., 2015). Other countries in the Gulf of Guinea are nevertheless affected by environmental problems. The DACCIWA (Dynamics-Aerosol-Chemistry-Cloud Interactions in West Africa; Knippertz et al., 2015) project conducted fieldwork in southern West Africa (SWA) in 2016 to investigate the impact of anthropogenic emissions, notably on air quality. One part of the project included airborne measurements of flaring emissions in order to fill the data gap on oil extraction activities in SWA. Those in situ measurements are, as far as we know, the first reported data on oil extraction activities in this region.

We use here the Lagrangian transport model FLEXPART (FLEXible PARTicle dispersion model; Stohl et al., 2005) in combination with an inventory of emissions dedicated to flaring emissions and created in the framework of the DACCIWA project (Deetz and Vogel, 2017) to reproduce the aircraft measurements. We focus on evaluating the sensitivity of the model to two parameters: the emission flux and the injection height of the flaring emissions. After a brief description of the DACCIWA project and the platform in Sect. 2, we present in Sect. 3 the model and the flaring emission inventory we used, as well as the estimation of the flaring plume injection height. We discuss the modeling results in Sect. 4.

2 The DACCIWA/APSOWA project

2.1 Description of the campaign

The EU-funded project DACCIWA focuses on the coupling between dynamics, aerosols, chemistry and clouds (Flamant et al., 2017). The research campaign was set up in June-July 2016 and undertook activities ranging from airborne measurements to running atmospheric numerical models. A map showing the location of the research site is presented in supplementary material (Fig. S1).

Our Atmospheric Pollution from Shipping and Oil Platforms of West Africa (APSOWA) project complementing DACCIWA seeks to characterize gaseous and particulate pollutants emitted by oil platforms off the coast of the Gulf of Guinea by dedicated flights conducted with the DLR (Deutsches Zentrum für Luft- und Raumfahrt) research aircraft Falcon-20.

Different instruments for gas and particulate measurements were deployed onboard. We focus on CO, NO_2, SO_2 and aerosols measurements during two flights on 10 and 14 July. Both CO and NO_2 were measured by SPIRIT (SPectromètre InfraRouge In situ Toute altitude, Catoire et al., 2017). This infrared absorption spectrometer uses continuous-wave distributed-feedback room-temperature Quantum Cascade Lasers (QCLs) allowing online scanning of mid-infrared rotational-vibrational lines

5   with spectral resolution of 10^{-3} cm^{-1}. In the present campaign, the ambient air is sampled in a multipass cell with a pathlength of 134.22 m and in micro-windows around the 2179.772 cm^{-1} line for CO and the 1630.326 cm^{-1} line for NO_2. A home-made software using the HITRAN 2012 database (Rothman et al., 2013) is used to deduce the total molecule abundance. The overall uncertainties are 4 ppbv for CO and 0.5 ppbv +5% for NO_2 at 1.6 s time resolution.

SO_2 measurements are performed using a pulsed fluorescence SO_2 analyser (Thermo Electron, Model 43C Trace Level).

10   Ultraviolet (UV) light is absorbed by SO_2 molecules in the sample gas which become excited and subsequently decay to a lower energy state. The emitted light is detected by a photomultiplier tube and is proportional to the SO_2 concentration in the sample gas. The time resolution of the measurements is 1 s, with a moving average of 30 s to smooth the data. The lower detection limit is 0.315 ppbv. The instrument was multipoint calibrated before and after the campaign.

Total aerosol concentrations were measured with a butanol-based condensation particle counter (CPC TSI 3010, modified

15   for aircraft use; Schröder & Ström, 1997 and Fiebig et al., 2005). The particle counter was mounted inside the fuselage behind the Falcon isokinetic aerosol inlet. The large particle cutoff diameter imposed by the inlet has been found to be between 1.5 and 3 μm depending on flight altitude (Fiebig, 2001). The lower cutoff diameter of the CPC was at ~10 nm. Particle losses due to diffusion effects were minimized by using a 5.75 std l/min bypass flow to the instrument. Using the particle loss calculator described in von der Weiden et al. (2009) we estimate the particle losses in the tubing to be less than

20   10% for the relevant size range. Flight sequences inside clouds are known to cause sampling artefacts and have therefore been removed from the data set.

2.2 Flight planning and FPSO description

The first Floating Production Storage and Offloading (FPSO) vessels have been installed in Indonesia in 1974. Since this year, their number has steadily increased (Shimamura, 2002). The concept of those platforms based on ship structure makes

25   possible the development of small size oil fields and/or in deeper water (Shimamura, 2002). Those platforms have other advantages (Shimamura, 2002): they are faster to build than other floating structures, they have inbuilt storage capability and thus do not necessitate pipelines, and they are movable and easily implantable on another oil field. Because of all those reasons, the FPSO systems will continue to develop. Among the techniques used to eliminate the gas associated with the crude oil extraction, one is the flaring, consisting in burning the gas in an open flame through a stack. This leads to a mixture

30   of gas which can reach the free troposphere if the meteorological conditions are favorable (Fawole et al., 2016b). The two targeted flights, on July 10 and July 14, consisted in about 3-4 hours of meandering transects through emission plumes in the MBL about 300 m above sea level (asl) off the coast of West Africa from Ivory Coast to Togo. We focus on the flights in the vicinity of the FPSO Kwame Nkrumah platform, on the Jubilee Field, off the coast of Ghana (4°35'47.04 N, 2°53'21.11 W).

It measures 330 m in length by 65 m in width, and its height up to the top of the chimney is estimated to be 112 m asl. During the campaign, no contact with this FPSO could be obtained in order to have more information on its functioning.

3 Method

3.1 Lagrangian particle dispersion modelling

5

The Lagrangian model FLEXPART (FLEXible PARTicle; Stohl et al., 2005) is used to study the transport of the emitted plume from the FPSO in the MBL. It simulates long-range transport and dispersion of atmospheric tracers released along time by computing trajectories of a large number of particles. Model calculations are based on meteorological data from the European Centre for Medium-Range Weather Forecasts (ECMWF), ERA-INTERIM L137 (Dee et al., 2011) extracted every

10   3 hours and with a horizontal grid mesh size of 0.5°×0.5°. The calculations are performed in forward dispersion mode with the model version 9.0. In this mode, each particle is associated to a given mass of tracer released during the time of the simulation. At the end of the simulation, the particles can be counted on a grid to estimate the mixing ratio from the source of emission. The molecules are released using constant emissions from Deetz and Vogel (2017) inventory during 7 h with a spin-up of 5 h, allowing the model to be balanced independently from the initial conditions. During the simulation, the NO_2

15   mass is lost by wet and dry deposition and by OH reaction (concentrations from GEOS-CHEM model; Technical note FLEXPART v8.2, http://flexpart.eu/downloads/26), which allows a lifetime of about 3 h at 298 K in the MBL.

3.2 Flaring emission inventory

20   Our study is based on a new gas-flaring emission inventory developed for DACCIWA project (Deetz and Vogel, 2017). This inventory provides emissions of CO, CO_2, NO, NO_2 and SO_2 for June-July 2014 and 2015 and we use a 2016 updated version for the period of the APSOWA-DACCIWA campaign. It is based on remote sensing observations using VIIRS nighttime radiant heat in combination with combustion equations from Ismail and Umukoro (2014). The emission estimation method is described in detail in Deetz and Vogel (2017). Only the assumptions of interest for our study are indicated: first,

25   the natural gas composition includes H_2S (Sonibare and Akeredolu, 2004). Second, this composition measured in the Niger Delta is valid for West Africa in general. Third, the source temperature is deduced from the VIIRS measurements on a monthly mean. For the FPSO platform, it is set to 1600 K, which is a good order of magnitude since the flame temperature can be as high as 2000 K (Fawole et al., 2016b). The CO, SO_2 and NO_2 fluxes estimated with this method for our two days of interest for the FPSO platform are 1.1×10^{-1}, 4.23×10^{-5} and 7×10^{-2} kg s^{-1}, respectively. Note that the highest uncertainties

30   (+33; -79%) associated to the estimation of gas flaring emissions arise from the parameters required in the combustion equations, e.g. the gas composition, the source temperature and the flare characteristics.

3.3 Estimation of the flaring plume injection height

The oil flaring emissions are generally emitted at higher temperatures than the temperature of the surrounding environment, which implies an important role for the buoyancy at the stack exit. The buoyancy and momentum effects raise the plume above its initial injection height and can lead to a source height that can be several times higher than the real height of the stack (Arya, 1999). The calculation required to determine the rise of a plume depends on the wind conditions and the

5   atmospheric stability. Before determining those parameters, we determine the MBL height that defines in which part of the troposphere we flew. The MBL is about 680 m asl on July 10 and 582 m asl on July 14 according to the European (ECMWF) and US (NCEP) operational forecasts. The wind conditions are determined by the Falcon-20 measurement system. An average of the wind speed measurements is calculated during the flight period in the vicinity of the platform (see Sect. 4.1). For July 10, an 8 minute mean wind speed of 9.4 ± 0.5 m s^{-1} has been calculated, where the standard deviation

10   represents the natural variability, which is larger than the measurement uncertainty. For July 14, a 7 minute wind speed mean of about 6.6 ± 0.7 m s^{-1} has been calculated. Thus, for both days the conditions are windy.

Concerning the potential temperature for July 10 and 14, the atmosphere is considered as stable with a positive potential temperature gradient. With respect to the two effects mentioned earlier, only the buoyancy is taken into account as the momentum can be neglected for such high temperature plume (Briggs, 1965). With all the previous parameters defined, it is

15   possible to calculate the plume injection height ΔH (in m) by using Eq. (1) reported by Briggs (1965, 1984):

$$\Delta H = 2.6(\frac{F_b}{us})^{1/3} \tag{1}$$

with F_b as the buoyancy effect in m^4 s^{-3} as defined in Eq. (2), u as the wind speed (in m s^{-1}) and s as the stability parameter in s^{-2} defined in Eq. (3) (Briggs, 1965):

$$F_b = g \frac{\Delta T}{T_s} w r^2 \tag{2}$$

20

$$s = \frac{g}{T}\left(\frac{\partial T}{\partial z}\right) + \Gamma \tag{3}$$

T, T_s, w and r are the absolute temperature of the ambient air, the absolute temperature of the stack gases, the vertical velocity of the effluent at the stack exit and the radius of the stack, respectively. ΔT is the difference between the two

25   temperatures. In Eq. (3), g is the gravitational acceleration, z the altitude and Γ the adiabatic lapse rate. Both the temperature at the stack exit and the effluent velocity are taken from Deetz and Vogel (2017). The calculated plume injection height ΔH is 27 m for July 10 and 14. Briggs' algorithm underestimates plume rise in stable atmospheric condition (Akingunola et al., 2018). Therefore, another method has been tested to determine the injection height, based on VDI 3782 (1985). For a stable atmosphere, the injection height ΔH (in m) of the plume is determined by Eq. (4):

30     $$\Delta H = 74.4 \times Q^{0.333} \times u^{-0.333} \tag{4}$$

with u as the wind speed in m s^{-1} and the unit of the coefficient (74.4) in s^4 kg^{-1} m^{-2}. The heat flow Q (Eq. 5) is defined in Deetz and Vogel (2017) as:

$$Q = H \cdot \frac{1}{f} \tag{5}$$

with H as the radiant heat observed by VIIRS and f as the fraction of radiated heat equals to 0.27 (Guigard et al., 2000). The calculated plume injection heights are, according to eq. 4, 68 m and 77 m for July 10 and 14, respectively.

4 Results and discussion

4.1 Description of the measurements

Figure 1 presents the part of the flights in the vicinity of the FPSO platform. During the flight on July 10, the flaring plume was crossed several times (Fig. 1a). It led to four NO_2 peaks between 12:33 and 12:45 UTC at an altitude of around 300 m (Fig. 1c). Four simultaneous peaks of aerosols were measured (Fig. 1c). No simultaneous CO peaks, neither SO_2 peaks (not shown) were detected in the plume of the FPSO platform for this flight. No peak was measured during a second series of transect at a higher altitude (around 600 m, Fig. 1a).

During the flight on July 14, three NO_2 peaks were measured during the first transects between 10:48 and 11:00 UTC at around 300 m of altitude downwind the FPSO vessel (Fig. 1b). Those peaks were simultaneously measured with aerosol and CO peaks (Fig. 1d), but no SO_2 was detected. This suggests that H_2S was not present in the natural gas composition for this oil rig. Thus, the natural gas composition given by Deetz and Vogel (2017) for the Niger Delta seems to be different from that in Ghana for those two flights. The presence (or no) of CO peaks is discussed in Sect. 4.3.

4.2 FLEXPART simulations of the flaring emissions

In order to confirm that the peaks detected by the aircraft instruments correspond to the flaring emissions from the platform and to simulate them, forward trajectories are calculated using FLEXPART. First, as a reference, a simulation called "control run" (CTRL) is run, in which the NO_2 flux for the FPSO platform is taken from Deetz and Vogel (2017), i.e. 7×10^{-2} kg s^{-1}, and the injection height is 27 m, calculated with Briggs' method (see Sect. 3.3).

A comparison of the wind speed and direction between ECMWF simulations and the Falcon measurements is presented in supplementary material. The wind speed and direction derived from ECMWF agree within 1 m s^{-1} and ~1.8°, respectively, for July 10 (Fig. S2) and within ~1 m s^{-1} and ~7°, respectively, for July 14 (Fig. S3). So the transport is well reproduced in FLEXPART. Figure 2a compares observed and simulated time series of NO_2 concentrations for the flight on July 10. The four measured peaks are all remarkably well reproduced in time by FLEXPART. Another study by Tuccella et al. (2017), using WRF-Chem, was able to reproduce the simulated peaks simultaneously to the measured ones for oil facilities emissions in the Norwegian Sea. A NO_2 background concentration has been added to the last two peaks. This background is representative of the ambient pollution not taken into account in FLEXPART as this model only simulates the pollution coming from the platform. However, the simulated concentrations are always underestimated, as also presented in Table 1 for the CTRL run, with the percentages representing the relative differences with respect to SPIRIT measurements.

Concerning the second and the fourth peak (Fig. 2a), the measurements show two close peaks that FLEXPART cannot simulate individually, leading to a single broader and less intense peak. This is probably due to the fact that the wind field grid mesh size of 0.5°×0.5° (see Sect. 3.1) is too coarse compared to the measurements. Even with a finer wind field grid mesh of 0.125°×0.125° (simulation not shown) such close peaks cannot be distinguished, suggesting a still insufficient spatial resolution. Figure 2d also compares the observed and simulated NO_2 concentrations for the flight on July 14. The simulation gives three peaks concomitant with the three measured peaks of interest. As for the first flight, all the peaks are underestimated by FLEXPART (Table 1).

Figures 2 b and e show the NO_2 plume simulated with FLEXPART as a function of distance from the source and altitude on July 10 and 14, respectively. The aircraft measurements, represented by the colored circles, are located at the upper part of the plume, away from the strongest concentrations. The work carried out is thus limited by the flight trajectories which were too high and too far from the FPSO platform to catch the part of the plume with the highest concentrations. The operational conditions during the flights were complex for the pilots, and safety concerns forced us to respect a minimum flight level (300 m) and a minimum distance from the source.

To understand the underestimation of the simulated concentrations and to better reproduce the measurements, several sensitivity tests were performed (Table 2). This allowed evaluating the sensitivity of the model to the injection height and to the flux. For this, we used the injection heights calculated with VDI 3782 method (1985; Sect. 3.3). As far as we know, no other inventory can provide an estimation of the flux of this FPSO platform. We thus decided to test the sensitivity of the model to a doubled flux. The results of these simulations are presented in Table 1.

On July 10, increasing the injection height (ST1) still leads to an underestimation of the concentrations compared to the measurements (Table 1). When doubling the flux (ST2), two peaks are overestimated and two underestimated. Finally, modifying both the injection height and the flux (ST3) lead to three peaks out of four overestimated. Globally, run ST2 presents the smallest differences on average with the measurements showing that simulations are sensitive to the flux. On July 14, ST1 simulation leads to an underestimation of each peak. ST2 simulation presents two peaks underestimated and one peak with the right concentration. The contrary is observed for ST3 with two peaks out of three overestimated. The smallest differences are for ST3, which means that the simulations are sensitive to both parameters. We can use the best simulation on each day to estimate the percentage of pollutants transported inside and above the MBL. In both cases, more than 90% of the pollutants are inside the MBL meaning that only a few quantities of pollutants reaches the free troposphere and is transported toward the population living along the coastline. Finally, we found that the NO_2 concentration difference between the measurements and simulations does not depend on the distance from the source.

We performed CO simulations as CO peaks were measured in one case out of two (Fig. 2c and 2f). For those simulations, we used the injection height of 27 m of the CTRL run and the flux from Deetz and Vogel (2017) of 1.1×10^{-1} kg s^{-1}. For the flight on July 10, FLEXPART simulates four CO peaks concomitant with the four NO_2 peaks while no increase in CO has been observed. On July 14, three peaks of CO are simulated at the same time as the three measured ones, but underestimated. CO

is always included as a gas emitted from flaring in the inventory for this specific vessel while it does not seem to be the case each time. A discussion on the flaring combustion processes is presented below.

4.3 Combustion processes involved in oil flare

5 From a combustion point of view, flares generate non-premixed highly turbulent flames, characterized by high-frequency fluctuating flow fields. Flares can be air-assisted or steam-assisted in order to achieve a better efficiency. The turbulence allows boosting the mixing and affects the chemical reaction process. Very recent attempts to model such flames (Aboje et al., 2017; Damodara et al. 2017) showed the influence of the composition of the natural gas and the validity of the chemical kinetic mechanism are of primary importance to predict the emitted species. Moreover, the flame characteristics such as

10 temperature, height, and length, have a strong impact on the dispersion of the plume together with wind speed and other meteorological variables (Rahnama et al., 2016). All these parameters need to be taken into account when considering air field campaigns.

McDaniel (1983) showed CO emissions are strongly related to flare efficiency. When the efficiency is ca. 99.8%, CO is below 10 ppmv, while CO emissions may reach 250 ppmv when the efficiency drops to 70%. CO emissions are clearly

15 linked to the quality of the combustion, which is directly impacted by the turbulence. The observed difference between July 10 and 14 in terms of CO emissions might be explained by: first, a lower wind speed on July 14 (see Sect. 3.3), so that less O_2 was available to burn with natural gas, and second, more disturbed weather conditions on July 14, as can be seen from the much more dispersed plume in Fig. 1b, resulting in fuel-rich pockets favoring CO formation. The results of this campaign should help to improve computational flare fluid dynamics modeling.

20

5 Conclusions

This study was conducted in the framework of the DACCIWA FP7 European project in July 2016 in southern West Africa. One target of the project was to measure emissions from oil rigs, which were not well estimated until then. With two flights planned in the vicinity of a FPSO platform, we reported the first flaring in-situ measurements in this region. The aim of this

25 work was to evaluate the capacity of FLEXPART model to reproduce the NO_2 airborne measurements and to evaluate the inventory of Deetz and Vogel (2017) in the case of point sources of pollution such as oil platforms. The injection height of the plume was estimated by performing different calculations. Finally, after several sensitivity runs, it appears that the flux must be increased in one case, and both the flux and the injection height have to be increased in the other case, to better reproduce the measurements. An estimation of the pollutant distribution above or inside the MBL shows that the pollutants

30 stay mainly inside the MBL, limiting the transport to the coastline. Sources of uncertainties are associated with the different calculations and hypotheses but the work is mainly limited by the flights trajectories, too far and too high from the platform. So it remains necessary to better quantify the emissions released during the flaring processes, locally but also at wider scales. Generally speaking, the satellite flaring inventory used in our study provides reasonable estimates of emissions, which suggests that for flights planned in the heart of a flaring plume, it will be possible to link the flaring observations obtained by

satellites with the emissions deduced from the airborne measurements. If this relationship is possible, a general relationship between the emissions and the radiant heat could thus allow estimating the emissions of all flaring processes detected by satellite.

References

Aboje, A. A., Hughes, K. J., Ingham, D. B., Ma, L., Williams, A., and Pourkashanian, M.: Numerical study of a wake-stabilized propane flame in a cross-flow of air, Journal of Energy Institute, 90, 145–158. http://dx.doi.org/10.1016/j.joei.2015.09.002, 2017.

25

Akingunola, A., Makar, P. A., Zhang, J., Darlington, A., Li, S.-M., Gordon, M., Moran, M. D., and Zheng, Q.: A chemical transport model study of plume-rise and particle size distribution for the Athabasca oil sands, Atmos. Chem. Phys., 18, 8667-8688, https://doi.org/10.5194/acp-18-8667-2018, 2018.

30 Anomohanran, O.: Determination of greenhouse gas emission resulting from gas flaring activities in Nigeria. Energy Policy, 45, 666–670. https://doi.org/10.1016/j.enpol.2012.03.018, 2012.

Arya, S. P.: Air Pollution Meteorology and Dispersion, Oxford University Press, 1999.

Asuoha, A. N., and Osu Charles, I.: Seasonal variation of meteorological factors on air parameters and the impact of gas flaring on air quality of some cities in Niger Delta (Ibeno and its environs), African Journal of Environmental Science and Technology, 9(3), 218–227. https://doi.org/10.5897/AJEST2015.1867, 2015.

5

Briggs, G. A.: A Plume Rise Model Compared with Observations, Journal of the Air Pollution Control Association, 15(9), 433–438, https://doi.org/10.1080/00022470.1965.10468404, 1965.

Briggs, G. A.: Plume rise and buoyancy effects, atmospheric sciences and power production, in: DOE/TIC-27601
10 (DE84005177), edited by: Randerson, D., TN, Technical Information Center, U.S. Dept. of Energy, Oak Ridge, USA, 327–366, 1984.

Brissebrat, G., Belmahfoud, N., Cloché, S., Ferré, H., Fleury, L., Mière, A., and Ramage, K.: The BAOBAB data portal and DACCIWA database, 19th EGU General Assembly, EGU2017, 23–28 April, 2017, Vienna, Austria, p. 4685, available at:
15 http://baobab.sedoo.fr/DACCIWA/ (last access: July 2018), 2017.

Catoire, V., Robert, C., Chartier, M., Jacquet, P., Guimbaud, C., and Krysztofiak, G.: The SPIRIT airborne instrument: a three-channel infrared absorption spectrometer with quantum cascade lasers for in situ atmospheric trace-gas measurements, Appl. Phys. B., 123(9), 244, https://doi.org/10.1007/s00340-017-6820-x, 2017.

20

Damodara, V., Chen, D. H., Lou, H. H., Rasel, K. M. A., Richmond, P., Wang, A., and Li, X.: Reduced combustion mechanism for C_1–C_4 hydrocarbons and its application in computational fluid dynamics flare modelling, Journal of the Air & Waste Management Association, 67(5), 599–612, https://doi.org/10.1080/10962247.2016.1268546, 2017.

25 Dee, D. P., Uppala, S. M., Simmons, A. J., Berrisford, P., Poli, P., Kobayashi, S., Andrae, U., Balmaseda, M. A., Balsamo, G., Bauer, P., Bechtold, P., Beljaars, A. C. M., van de Berg, L., Bidlot, J., Bormann, N., Delsol, C., Dragani, R., Fuentes, M., Geer, A. J., Haimberger, L., Healy, S. B., Hersbach, H., Hólm, E. V., Isaksen, L., Kållberg, P., Köhler, M., Matricardi, M., McNally, A. P., Monge-Sanz, B. M., Morcrette, J.-J., Park, B.-K., Peubey, C., de Rosnay, P., Tavolato, C., Thépaut, J.-N., and Vitart, F.: The ERA-Interim reanalysis: configuration and performance of the data assimilation system, Q.J.R. Meteorol.
30 Soc., 137, 553–597, doi:10.1002/qj.828, 2011.

Deetz, K., and Vogel, B.: Development of a new gas-flaring emission dataset for southern West Africa, Geosci. Model Dev., 10(4), 1607–1620, https://doi.org/10.5194/gmd-10-1607-2017, 2017.

35 Elvidge, C. D., Zhizhin, M., Hsu, F.-C., and Baugh, K. E.: VIIRS Nightfire: Satellite Pyrometry at Night, Remote Sensing, 5(9), 4423–4449, https://doi.org/10.3390/rs5094423, 2013.

Elvidge, C. D., Zhizhin, M., Baugh, K., Hsu, F.-C., and Ghosh, T.: Methods for Global Survey of Natural Gas Flaring from Visible Infrared Imaging Radiometer Suite Data, Energies, 9(1), 14. https://doi.org/10.3390/en9010014, 2015.

40

Fawole, O. G., Cai, X., Levine, J. G., Pinker, R. T., and MacKenzie, A. R.: Detection of a gas flaring signature in the AERONET optical properties of aerosols at a tropical station in West Africa, Journal of Geophysical Research: Atmospheres, 121(24), 2016JD025584, https://doi.org/10.1002/2016JD025584, 2016a.

45 Fawole, O. G., Cai, X.-M., and MacKenzie, A. R.: Gas flaring and resultant air pollution: A review focusing on black carbon, Environmental Pollution, *216*, 182–197, https://doi.org/10.1016/j.envpol.2016.05.075, 2016b.

Fiebig, M.: Das troposphärische Aerosol in mittleren Breiten - Mikrophysik, Optik und Klimaantrieb am Beispiel der Feldstudie LACE 98, Ph.D. thesis, Ludwig-Maximilians-Universität, 2001.
50

Fiebig, M., Stein, C., Schroder, F., Feldpausch, P., and Petzold, A.: Inversion of data containing information on the aerosol particle size distribution using multiple instruments, Journal of Aerosol Science, 36(11): 1353, DOI:10.1016/j.jaerosci.2005.01.004, 2005.

5   Flamant, C., Knippertz, P., Fink, A. H., Akpo, A., Brooks, B., Chiu, C. J., et al.: The Dynamics-Aerosol-Chemistry-Cloud Interactions in West Africa field campaign: Overview and research highlights, Bulletin of the American Meteorological Society, https://doi.org/10.1175/BAMS-D-16-0256.1, 2017.

Guigard, S. E., Kindzierski, W. B., and Harper, N.: Heat Radiation from Flares. Report prepared for Science and Technology
10   Branch, Alberta Environment, ISBN 0-7785-1188-X, Edmonton, Alberta, 2000.

Hassan, A., and Kouhy, R.: Gas flaring in Nigeria: Analysis of changes in its consequent carbon emission and reporting, Accounting Forum, 37(2), 124–134, https://doi.org/10.1016/j.accfor.2013.04.004, 2013.

15   Ismail, O. S., and Umukoro, G. E.: Modelling combustion reactions for gas flaring and its resulting emissions, Journal of King Saud University - Engineering Sciences, 28(2), 130–140, https://doi.org/10.1016/j.jksues.2014.02.003, 2016.

Knippertz, P., Coe, H., Chiu, J. C., Evans, M. J., Fink, A. H., Kalthoff, N., Liousse, C., Mari, C., Allan, R.P., Brooks, B., Danour, S., Flamant, C., Jegede, O.O., Lohou, F., and Marsham, J.H.: The DACCIWA Project: Dynamics–Aerosol–
20   Chemistry–Cloud Interactions in West Africa, B. Am. Meteorol. Soc., 96(9), 1451–1460, https://doi.org/10.1175/BAMS-D-14-00108.1, 2015.

McDaniel, M.: Flare efficiency study, Available http://www.epa.gov/ttn/chief/ap42/ch13/related/ref_01c13s05_jan1995.pdf (last access: July 2018), 1983.
25
Nwankwo, C. N. and Ogagarue, D. O.: Effects of gas flaring on surface and ground waters in Delta State Nigeria, Journal of Geology and Mining Research, 3, 131–136, 2011.

Nwaugo, V. O., Onyeagba, R. A., and Nwahcukwu, N. C.: Effect of gas flaring on soil microbial spectrum in parts of Niger
30   Delta area of southern Nigeria, African Journal of Biotechnology, 5, 1824–1826, 2006.

Osuji, L. C. and Avwiri, G. O.: Flared Gas and Other Pollutants Associated with Air quality in industrial Areas of Nigeria: An Overview, Chem. Biodivers., 2, 1277–1289, 2005.

35   Rothman, L. S., Gordon, I. E., Babikov, Y., Barbe, A., Chris Benner, D., Bernath, P. F., Birk, M., Bizzocchi, L., Boudon, V., Brown, L. R., Campargue, A., Chance, K., Cohen, E. A., Coudert, L. H., Devi, V.M., Drouin, B. J., Fayt, A., Flaud, J.-M., Gamache, R. R., Harrison, J. J., Hartmann, J.-M., Hill, C., Hodges, J. T., Jacquemart, D., Jolly, A., Lamouroux, J., Le Roy, R. J., Li, G., Long, D. A., Lyulin, O. M., Mackie, C. J., Massie, S. T., Mikhailenko, S., Müller, H. S. P., Naumenko, O. V., Nikitin, A. V., Orphal, J., Perevalov, V., Perrin, A., Polovtseva, E. R., Richard, C., Smith, M. A. H., Starikova, E., Sung, K.,
40   Tashkun, S., Tennyson, J., Toon, G. C., Tyuterev, Vl. G., and Wagner, G.: The HITRAN2012 molecular spectroscopic database, Journal of Quantitative Spectroscopy and Radiative Transfer, 130, 4-50, ISSN 0022-4073, doi:10.1016/j.jqsrt.2013.07.002, 2013.

Shimamura, Y.: FPSO/FSO: State of the art, Journal of Marine Science and Technology, 7(2), 59–70,
45   https://doi.org/10.1007/s007730200013, 2002.

Rahnama, K., and De Visscher, A.: Simplified Flare Combustion Model for Flare Plume Rise Calculations, The Canadian Journal of Chemical Engineering, 94, 1249–1261, 2016.

Schröder, F. and Ström, J.: Aircraft measurements of sub micrometer aerosol particles (> 7 nm) in the midlatitude free troposphere and tropopause region, Atmospheric Research, 44(3-4): 333, DOI:10.1016/S0169-8095(96)00034-8, 1997.

Sonibare, J. A., and Akeredolu, F. A.: A theoretical prediction of non-methane gaseous emissions from natural gas combustion, Energy Policy, 32(14), 1653–1665, https://doi.org/10.1016/j.enpol.2004.02.008, 2004.

Stohl, A., Forster, C., Franck, A., Seibert, P., and Wotawa, G.: Technical note : The Lagrangian particle dispersion model FLEXPART version 6.2. Atmos. Chem. Phys., *5*, 2461–2474, https://doi.org/1680-7324/acp/2005-5-2461, 2005.

Tuccella, P., Thomas, J. L., Law, K. S., Raut, J.-C., Marelle, L., Roiger, A., Weinzierl, B., Denier van der Gon, H.A.C., Schlager, H., and Onishi, T.: Air pollution impacts due to petroleum extraction in the Norwegian Sea during the ACCESS aircraft campaign, Elem Sci Anth, 5(0), https://doi.org/10.1525/elementa.124, 2017.

VDI 3782: Dispersion of Air Pollutants in the Atmosphere, Determination of Plume rise. Verein Deutscher Ingenieure, VDI-Richtlinien 3782 Part 3, 1985.

Vogel, B., Vogel, H., Bäumer, D., Bangert, M., Lundgren, K., Rinke, R., and Stanelle, T.: The comprehensive model system COSMO-ART – Radiative impact of aerosol on the state of the atmosphere on the regional scale, Atmos. Chem. Phys., 9(22), 8661–8680, https://doi.org/10.5194/acp-9-8661-2009, 2009.

von der Weiden, S. L., Drewnick, F., and Borrmann, S.: Particle Loss Calculator – a new software tool for the assessment of the performance of aerosol inlet systems, Atmos. Meas. Tech.*,* 2(2): 479, DOI:10.5194/amt-2-479-2009, 2009.
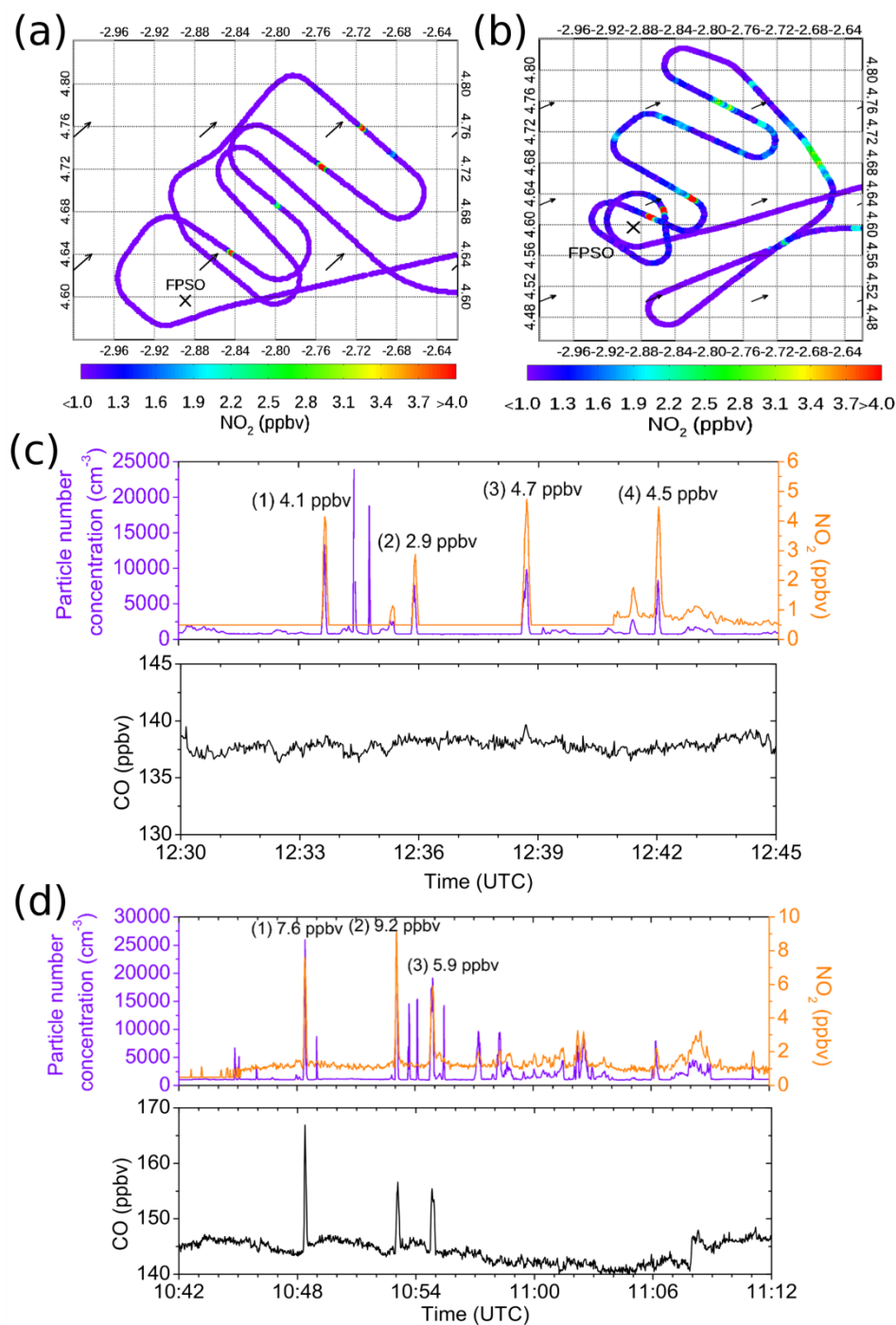
Figure 1: (a) NO₂ concentration as a function of the flight trajectory downwind of the FPSO plume for July 10. The black arrows show the wind direction (from ECMWF). (c) NO₂, aerosol, and CO concentrations as a function of time zoomed in a part of the flight trajectory in (a). The peaks studied are labelled by a number (from 1 to 4). (b) and (d) are similar to (a) and (c) for July 14.
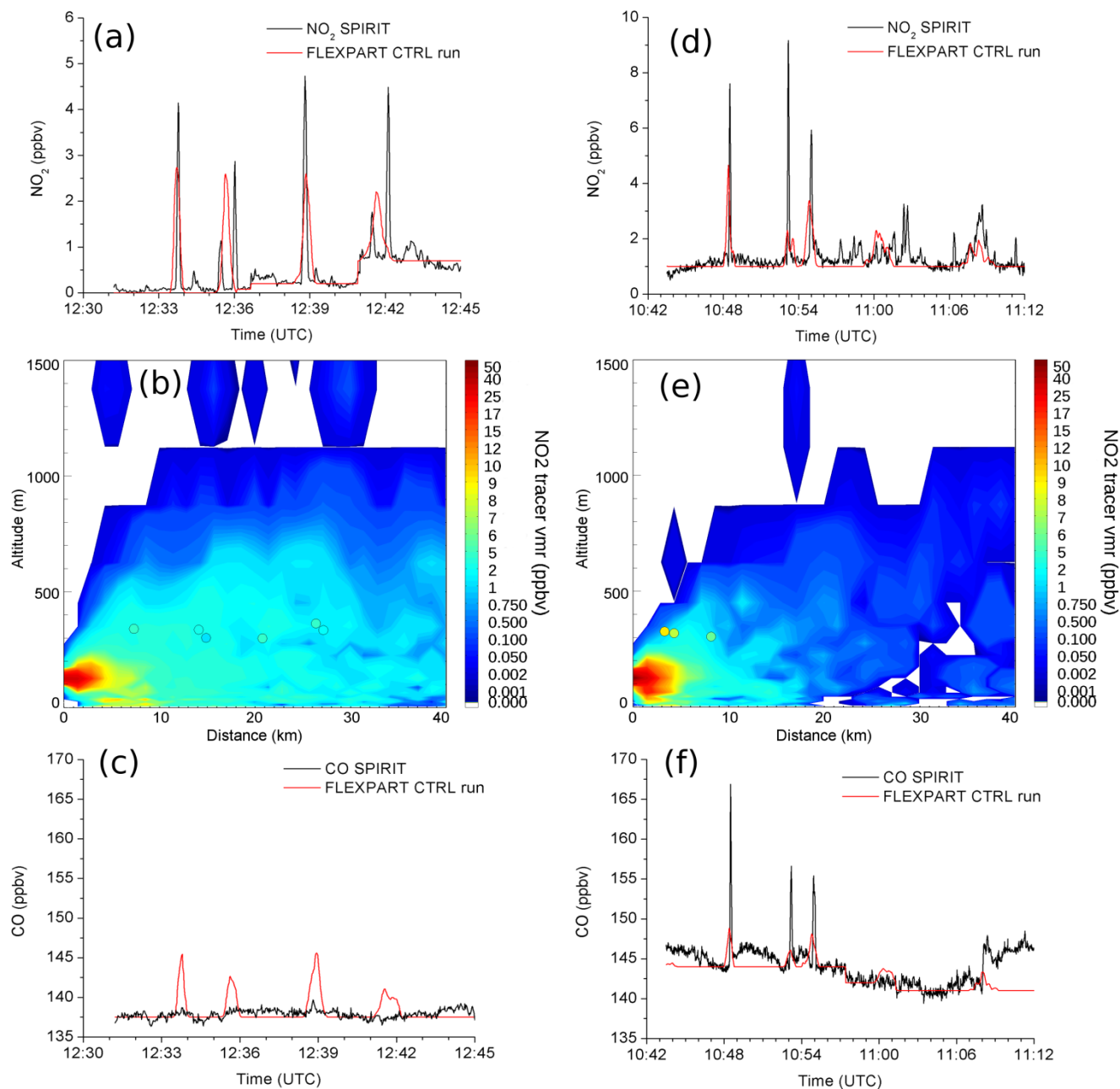
5

Atmospheric
Chemistry
and Physics
Discussions

Figure 2. Left column: July 10. (a) NO$_2$ concentration as a function of time for SPIRIT measurements (black) and FLEXPART CTRL run simulation (red). (b) Vertical section of the simulated NO$_2$ plume (CTRL run) as a function of distance from the source and altitude. The colored circles correspond to the measurement peaks. (c) CO concentration as a function of time for measurements (black) and FLEXPART CTRL run simulation (red). Right column: July 14. (d), (e) and (f) similar to (a), (b) and (c).

Atmospheric
Chemistry
and Physics
Discussions

Date	Distance (km)	Altitude (m)	SPIRIT (ppbv)	CTRL (ppbv)	ST 1 (ppbv)	ST 2 (ppbv)	ST 3 (ppbv)
20160710	7.2	339.7	4.1±0.7	2.7 (-34.1%)	3.1 (-24.4%)	5.9 (+33.9%)	6.3 (+53.7%)
	14.5	335.9	2.9±0.6	2.6 (-10.3%)	1.7 (-41.4%)	5.8 (+100.0%)	3.7 (+27.6%)
	21.0	298.7	4.7±0.7	2.6 (-44.7%)	2.6 (-44.7%)	2.9 (-38.3%)	5.2 (+10.6%)
	27.0	362.9	4.5±0.7	2.2 (-51.1%)	2.7 (-40.0%)	2.6 (-42.2%)	4.1 (-8.9%)
20160714	4.6	318.7	7.6±0.8	4.7 (-38.2%)	5.1 (-32.9%)	6.4 (-15.8%)	11.9 (+36.1%)
	2.7	326.0	9.2±0.9	2.3 (-75.0%)	4.5 (-51.1%)	4.4 (-52.2%)	6.7 (-27.2%)
	8.8	303.7	5.9±0.7	3.4 (-42.4%)	4.4 (-25.4%)	5.9 (0%)	6.5 (+10.2%)

Table 1. NO$_2$ concentrations measured with SPIRIT and simulated in CTRL run, and sensitivity tests (ST) for July 10 and July 14. The distances from the platform and the altitudes of the aircraft are reported. The percentages represent the differences with respect to SPIRIT measurements.

5

Run name	Date of flight	Flux	Injection height
CTRL	20160710	0.07 kg s^{-1}	27 m
	20160714		
ST1	20160710	0.07 kg s^{-1}	68 m
	20160714	0.07 kg s^{-1}	77 m
ST2	20160710	0.14 kg s^{-1}	27 m
	20160714		
ST3	20160710	0.14 kg s^{-1}	68 m
	20160714	0.14 kg s^{-1}	77 m

Table 2. Flux and injection height for the reference control run (CTRL) and for the sensitivity tests (ST) for each day of flight.